JOURNAL OF GUIDANCE, CONTROL, AND DYNAMICS
Vol. 26, No. 2, March–April 2003

Prediction Tools for Active Damping and Motion Planning of Flexible Manipulators

B. Pond* and J. Van Vliet*
University of Victoria, Victoria, British Columbia V8W 3P6, Canada
and
I. Sharf†
McGill University, Montreal, Quebec H3A 2K6, Canada

Three novel predictive tools are developed for motion planning and active damping of long-reach flexible manipulator systems. One of these, the momentum coupling map, is an enhancement of the previously proposed coupling map concept, extended to general flexible-link or flexible-joint manipulator systems. It is a graphical tool and can be used to optimize the motion of the flexible manipulator to minimize the vibration excited during a point-to-point maneuver. The other two, the accelerative damping map and the modal inertia map, were motivated by the active damping problem of macro–micro manipulators. They are designed to predict the optimal micromanipulator configuration for damping vibrations in the supporting (macro-) arm. The performance of the maps is illustrated by using two example manipulator systems: a simple two-link robot and the experimental macro–micro manipulator constructed at the University of Victoria. For motion planning, the paths predicted with the maps are compared with those calculated by the global optimization procedure. For active damping, the maps are compared and evaluated against the experimental results for the macro–micro arm. It is demonstrated that the observed damping performance is in very good agreement with the predictions of the maps.

I. Introduction

A MACRO–MICRO manipulator is a specialized robotic system comprising a large flexible arm with a short-reach rigid manipulator attached to its end. The macroarm provides large reach capability, whereas the small arm is used for fine dextrous manipulation. Two prominent examples of macro–micro manipulator systems are the space station remote manipulator system in combination with the special purpose dextrous manipulator (SSRMS/SPDM) and the light duty utility arm (LDUA). The SSRMS is being used in the construction of the International Space Station (SPDM is expected to be launched in 2004), whereas LDUA was designed for nuclear waste remediation. Note that the terms macro and micro used to describe these configurations primarily are intended to differentiate the functionality rather than the dimensions of the two robots.

The problem of motion planning for robotic arms with structural flexibility, and more specifically, macro–micro manipulators, involves determining the optimal path and speed in joint space that minimizes vibration excitation and residual vibrations. Active damping of macro–micro manipulators can be viewed as a complementary problem where the issue is how to use the microrobot to damp out the vibrations in the macroarm.

Both problems have been considered previously, and several solutions are available. For example, a few authors attempted some variation of a global optimization solution to determine optimal motion of a flexible manipulator with respect to a particular vibration objective. The procedure has been applied to optimize either the speed along a given joint path,[1] or joint accelerations for point-to-point tasks,[2,3] or parameterized point-to-point joint trajectories.[4,5] The objectives considered include residual vibration energy,[1] the energy of the higher harmonics in the required joint torques,[2,3] the norm of the elastic coordinates and rates,[4] and the global vibration energy.[5] Also for motion planning, one predictive technique, the coupling map, has been applied successfully to an experimental space manipulator.[6] The coupling map is a graphical tool and contains local information on the degree of coupling and directions of least coupling in joint space. It allows the user to plan heuristically the motion of the small robot to minimize the excitation of the flexible supporting structure.

A few solutions to the active damping problem have been described in literature. In an early work, Book and Lee[7] developed a dual-timescale approach with a "slow" controller used for the rigid coordinates and a "fast" controller dissipating elastic vibrations. Subsequently, they extended the theory and increased the efficiency of the algorithm for real-time implementation.[8] Experimental results were obtained with the Georgia Institute of Technology's RALF/SAM macro–micro manipulator. Trudnowski et al.[9] developed the inertial damping approach that was validated by using the large test facility at the Pacific National Laboratory.[10] The same approach, combined with command filtering techniques, was investigated further by Cannon et al.[11] Sharf[12] presented an active damping algorithm where the macro- and micromanipulators are decoupled through their interaction force. The micromanipulator joint motions are calculated to apply the desired damping reaction to the supporting flexible arm. A similar approach was pursued by Book and Loper.[13] Torres et al.[14] proposed a solution called the pseudo-passive energy dissipation, which does not require sensing the elastic state. The method was evaluated experimentally, demonstrating superior damping performance compared to a stiff proportional-derivative (PD) controller.

It is acknowledged by researchers who investigate the active damping problem that there exist certain optimal micromanipulator configurations where damping is most effective. However, little research effort has been directed at determining these optimal configurations.

In this paper, we present the development and application of three novel predictive tools for active damping and motion planning. Our motivation is twofold: 1) to provide some alternatives to the existing procedures for motion planning of flexible manipulators that are computationally less expensive but are sufficiently accurate for a range of applications and 2) to develop tools to predict optimal macromanipulator configurations for active damping. The first of these, the momentum coupling map, was motivated by the aforementioned coupling map and is applicable to generic robotic arms

Received 26 July 2001; revision received 19 May 2002; accepted for publication 12 October 2002.

*Graduate Student, Department of Mechanical Engineering.
†Associate Professor, Department of Mechanical Engineering; inna.sharf@mcgill.ca. Senior Member AIAA.

with flexible and rigid links and/or flexible joints. The accelerative damping map has its origin in the simplified elastic dynamics equations and can be used both for planning motions to minimize elastic vibration or for determining good micromanipulator configurations for active damping. The third map proposed in this paper, the modal inertia map, is motivated by the active damping scenario. It provides a measure of the sensitivity of the microrobot to macroarm vibrations. Following the derivation of the three maps, we present results demonstrating their performance using three example manipulators: a planar two-link robot, the same robot but with gravity included in the environment, and the experimental macro–micro manipulator at the University of Victoria. The paper is concluded with comments on the fidelity and viability of the three maps for the applications considered.

II. Prediction Tools

A. Momentum Coupling Map

As noted, the derivation of the momentum coupling map (MCM) was motivated by the coupling map concept originally proposed in Torres and Dubowsky.[15] The MCM derived here is more general because it is applicable to open-chain manipulator systems with flexible and rigid members and is not restricted to the macro–micro manipulator topology. The elastic deformation of the system is represented by $\boldsymbol{q}_e \in \boldsymbol{R}^s$, for example, finite element coordinates, and the manipulator joint angles are $\boldsymbol{q}_r \in \boldsymbol{R}^n$. Then the dynamics equations governing the motion of the manipulator can be stated in the following partitioned form:

$$\boldsymbol{M}_{rr}(\boldsymbol{q}_r, \boldsymbol{q}_e)\ddot{\boldsymbol{q}}_r + \boldsymbol{M}_{re}(\boldsymbol{q}_r, \boldsymbol{q}_e)\ddot{\boldsymbol{q}}_e + \boldsymbol{h}_r(\boldsymbol{q}_r, \boldsymbol{q}_e, \dot{\boldsymbol{q}}_r, \dot{\boldsymbol{q}}_e) = \boldsymbol{\tau} \quad (1)$$

$$\boldsymbol{M}_{er}(\boldsymbol{q}_r, \boldsymbol{q}_e)\ddot{\boldsymbol{q}}_r + \boldsymbol{M}_{ee}(\boldsymbol{q}_r, \boldsymbol{q}_e)\ddot{\boldsymbol{q}}_e + \boldsymbol{K}_e\boldsymbol{q}_e + \boldsymbol{h}_e(\boldsymbol{q}_r, \boldsymbol{q}_e, \dot{\boldsymbol{q}}_r, \dot{\boldsymbol{q}}_e) = \boldsymbol{0} \quad (2)$$

where the symmetric manipulator mass matrix $\boldsymbol{M}$ is partitioned as shown, $\boldsymbol{\tau}$ are the applied joint torques, $\boldsymbol{K}_e$ is the manipulator stiffness matrix, and $\boldsymbol{h}_r$ and $\boldsymbol{h}_e$ contain the nonlinear inertial terms and gravitational forces. To simplify the notation, the dependence of $\boldsymbol{M}$ on the generalized coordinates will be omitted henceforth.

To derive the MCM, we assume that the elastic components of the generalized momentum of the system are zero, and hence, the following relationship holds between elastic and rigid rates:

$$\boldsymbol{M}_{ee}\dot{\boldsymbol{q}}_e + \boldsymbol{M}_{er}\dot{\boldsymbol{q}}_r = \boldsymbol{0} \quad (3)$$

For small joint motions, Eq. (3) can be equivalently rewritten in differential form as

$$\delta\boldsymbol{q}_e = -\boldsymbol{M}_{ee}^{-1}\boldsymbol{M}_{er}\delta\boldsymbol{q}_r \quad (4)$$

Using the standard definition for the strain energy in the structure,

$$V = \tfrac{1}{2}\boldsymbol{q}_e^T\boldsymbol{K}_e\boldsymbol{q}_e \quad (5)$$

and expanding Eq. (5) in a truncated Taylor's series about $\boldsymbol{q}_e = \boldsymbol{0}$ gives, for constant stiffness $\boldsymbol{K}_e$,

$$V = \tfrac{1}{2}\delta\boldsymbol{q}_e^T\boldsymbol{K}_e\delta\boldsymbol{q}_e \quad (6)$$

Combining Eq. (6) with Eq. (4) yields the desired form of V:

$$V = \tfrac{1}{2}\delta\boldsymbol{q}_r^T\boldsymbol{Q}\delta\boldsymbol{q}_r \quad (7)$$

where the momentum coupling matrix is

$$\boldsymbol{Q} := \boldsymbol{M}_{er}^T\boldsymbol{M}_{ee}^{-T}\boldsymbol{K}_e\boldsymbol{M}_{ee}^{-1}\boldsymbol{M}_{er} \quad (8)$$

The coupling matrix derived here differs from that in Ref. 15 in two respects. First, it involves the stiffness matrix of the flexible structure, rather than its inverse, and second, it applies to general flexible manipulator systems. The largest eigenvalue of the coupling matrix $\boldsymbol{Q}$ indicates the degree of coupling between rigid motions and the strain energy induced in the flexible degrees of freedom. For macro–micro manipulator systems, these correspond to micromanipulator joint motions and the degrees of freedom of the flexible supporting arm. The eigenvector associated with the minimum eigenvalue provides a direction of least coupling, which is useful for path planning. Thus, the MCM is a graphical representation in the configuration space of regions of high relative coupling, indicated by darker shading, superimposed on lines showing the directions of least coupling (minimum coupling lines).

B. Accelerative Damping Map

The development of the accelerative damping map can be approached from two perspectives. In the context of active damping of macro–micro manipulators, one typically assumes small rigid and elastic rates. Then, only micromanipulator joint accelerations can apply appreciable forces and moments to the flexible macroarm, which in turn serve to damp the structural vibrations. For any micromanipulator joint accelerations $\ddot{\boldsymbol{q}}_r$ applied from rest, the resulting generalized force is

$$\boldsymbol{f}_e = \boldsymbol{M}_{er}\ddot{\boldsymbol{q}}_r \quad (9)$$

Alternatively, the same result can be deduced by using general dynamics equations (1) and (2). To this end, we rewrite the elastic dynamics equation (2) as

$$\boldsymbol{M}_{ee}\ddot{\boldsymbol{q}}_e + \boldsymbol{K}_e\boldsymbol{q}_e = -\boldsymbol{M}_{er}\ddot{\boldsymbol{q}}_r - \boldsymbol{h}_e \quad (10)$$

and interpret each term on the right-hand side as generalized forces applied to the elastic degrees of freedom. Assuming the $\ddot{\boldsymbol{q}}_r$ term to be the predominant forcing function leads to the same result as given in Eq. (9).

The strain energy, stated earlier in Eq. (5), can also be rewritten in terms of generalized forces by making use of the load-deflection relation $\boldsymbol{f}_e = \boldsymbol{K}_e\boldsymbol{q}_e$, where the stiffness matrix is positive definite. Then,

$$V = \tfrac{1}{2}\boldsymbol{f}_e^T\boldsymbol{K}_e^{-1}\boldsymbol{f}_e \quad (11)$$

and substituting for the generalized force from Eq. (9) yields

$$V = \tfrac{1}{2}\ddot{\boldsymbol{q}}_r^T\boldsymbol{M}_{er}^T\boldsymbol{K}_e^{-1}\boldsymbol{M}_{er}\ddot{\boldsymbol{q}}_r \quad (12)$$

Equation (12) represents the strain energy of the system resulting from rigid joint accelerations, under the assumption of small rates. From it, one can define the accelerative damping matrix as

$$\boldsymbol{Q}_A = \boldsymbol{M}_{er}^T\boldsymbol{K}_e^{-1}\boldsymbol{M}_{er} \quad (13)$$

For a macro–micro manipulator configuration described with $\boldsymbol{q}_r$ and $\boldsymbol{q}_e$, respectively, the eigenvalues of the accelerative damping matrix are indicative of the sensitivity of flexible (macro-) manipulator deflections to micromanipulator joint accelerations. Thus, if the eigenvalues are large, good active damping performance is predicted. The Euclidean norm of the vector of eigenvalues of $\boldsymbol{Q}_A$ is the scalar measure of predicted damping performance from the accelerative damping map. For motion planning, a map can be generated by using the largest eigenvalue and the minimum eigenvalue eigenvector of $\boldsymbol{Q}_A$ (over the configuration space), similarly to the MCM derived from $\boldsymbol{Q}$ of Eq. (8).

C. Modal Inertia Map

An alternative for predicting the optimal microrobot configurations for active damping, the modal inertia map (MIM), was proposed by Van Vliet.[16] This map is conceptually different from the other two maps presented here. For macro–micro manipulators, both the MCM and accelerative damping map give a measure of the strain energy induced in the macroarm as a result of the motion of the microrobot. By contrast, the MIM represents the sensitivity of micromanipulator joint motions to the macromanipulator's vibration. The map is motivated by the fact that, when the micromanipulator is configured such that it is sensitive to macroarm vibrations, good damping performance is expected. This sensitivity can be measured by the torque required to hold the micromanipulator joints in the nominal configuration $\bar{\boldsymbol{q}}_r$ as the macroarm vibrates.

This concept can be easily generalized to manipulators with flexible and rigid degrees of freedom. In particular, if the rigid

coordinates are fixed (joints are locked) and neglecting remaining nonlinearities, the dynamics equations for the system reduce to

$$\boldsymbol{M}_{re}\ddot{\boldsymbol{q}}_e = \boldsymbol{\tau} \tag{14}$$

$$\boldsymbol{M}_{ee}\ddot{\boldsymbol{q}}_e + \boldsymbol{K}_e\boldsymbol{q}_e = \boldsymbol{0} \tag{15}$$

from which the required "hold" torque is

$$\boldsymbol{\tau} = \boldsymbol{M}_{re}\ddot{\boldsymbol{q}}_e = -\boldsymbol{M}_{re}\boldsymbol{M}_{ee}^{-1}\boldsymbol{K}_e\boldsymbol{q}_e \tag{16}$$

If we further assume that the macromanipulator vibration is confined to the dominant mode $\bar{\boldsymbol{q}}_e$, then $\ddot{\boldsymbol{q}}_e = -\bar{\omega}_e^2\bar{\boldsymbol{q}}_e$, and the corresponding torque becomes

$$\bar{\boldsymbol{\tau}} = \bar{\omega}_e^2\boldsymbol{M}_{re}\bar{\boldsymbol{q}}_e \tag{17}$$

where $\bar{\omega}_e$ is the dominant natural frequency. The elements of $\bar{\boldsymbol{\tau}}$ are proportional to the effective inertia seen at each joint for vibration confined to the dominant elastic mode. The Euclidean norm of this torque is used to plot the MIM over the configuration space of the microrobot or over the range space of rigid degrees of freedom (DOF). In Sec. V, results calculated with MIM are compared with the accelerative damping map and experiment.

III. Example Systems

The first flexible manipulator used to illustrate the performance of the motion planning tools is called REMSPATIAL and was chosen as a convenient intuitive example. Its first link is rigid, whereas the second link is flexible with planar bending only (Fig. 1). A steel sphere at the tip of the flexible link acts as the payload. Table 1 lists the physical properties of the bodies. The flexible link is modeled by a single beam element, giving two elastic coordinates, the deflection and slope of the tip of the link.

Rotation of the second joint allows any orientation of the bending plane relative to the rotation plane of the first link. In particular, the bending plane of the flexible link can be oriented to decouple the link vibration from motion of the first joint. This configuration, thus, helps verify motion planning schemes by providing an intuitive solution for trajectories with minimal vibration excitation.

A modification of the REMSPATIAL example is introduced to illustrate further the limitations of the motion planning maps. We again consider the REMSPATIAL manipulator, but the environment is now modified to include gravity acting perpendicularly to the rotation plane of the first, rigid link. Thus, the orientation of the elbow joint determines the orientation of the flexible link relative to gravity. For example, when the elbow is in the 0-deg configuration, the bending plane is perpendicular to gravity (decoupled), but is parallel to gravity at ±90 deg (coupled). Without gravity, the coupling of vibration to shoulder joint acceleration displays the opposite characteristics, coupled when the elbow is at 0 deg, but decoupled at ±90 deg. The rotation of the elbow must, therefore, be planned according to the net force resulting from gravity and shoulder joint rotation.

Table 1 Physical properties[a] of REMSPATIAL

Body	Dimension, cm	Mass, kg
Rigid	53	0.8
Elastic	$50 \times 5 \times 0.6$	0.4
Sphere	13.4 diameter	10

[a]Stiffness of flexible link $EI = 74.7\ \mathrm{N \cdot m^2}$.

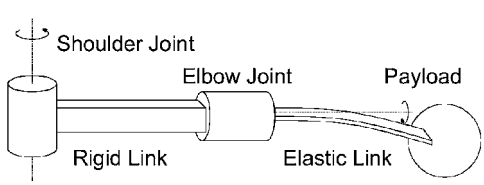

Fig. 1 REMSPATIAL manipulator.

The LAURA–SARA manipulator, shown in Fig. 2, was constructed in the Space and Subsea Robotics Laboratory at the University of Victoria specifically for experimental validation of active damping techniques for macro–micro manipulators.[17] (LAURA is an acronym for long articulated UVic robotic arm and SARA is an acronym for small articulated rigid arm.) This planar macro–micro manipulator is supported on a large glass table with air bearings under each joint to minimize friction with the table. LAURA consists of two flexible links actuated by two harmonic drive motors; SARA is a 3-DOF rigid robot actuated with direct-drive brushed dc motors. A detailed description of the macro–micro manipulator design, geometry, stiffness, and inertia properties may be founded in Van Vliet.[16]

IV. Application to Motion Planning

In this section, we employ the MCM and accelerative damping map to predict joint paths of least coupling. To evaluate the utility of the maps, we also present the optimal motion solution obtained with the global optimization procedure summarized briefly later.

A. Globally Optimal Solution

In Ref. 18, we developed a different path planning methodology that minimizes the undesirable elastic vibrations. The motion planning problem was formulated as a two-point boundary value problem that yields a globally optimal solution for the particular objective. The objective is written in the general form

$$\min_{u} J[\boldsymbol{u}] = f(T) + \int_0^T F(\boldsymbol{x}, \boldsymbol{u})\,\mathrm{d}t \tag{18}$$

where F is chosen to represent the strain energy of Eq. (5), $\boldsymbol{x}$ is the state of the manipulator dynamics, and the control input $\boldsymbol{u}$ is set to $\ddot{\boldsymbol{q}}_r$. The first term $f(T)$ enforces the constraint on $\boldsymbol{x}$ at the terminal time T. The optimization problem (18) is subject to the *nonlinear* dynamics equations, which can be summarized in first-order form as

$$\dot{\boldsymbol{x}} = \boldsymbol{f}(\boldsymbol{x}, \boldsymbol{u}) \tag{19}$$

$$\dot{\boldsymbol{x}} = \begin{pmatrix} \dot{\boldsymbol{q}}_r \\ \dot{\boldsymbol{q}}_e \\ \boldsymbol{u} \\ -\boldsymbol{M}_{ee}^{-1}\left(\boldsymbol{M}_{re}^T\boldsymbol{u} + \boldsymbol{K}_e\boldsymbol{q}_e + \boldsymbol{h}_e\right) \end{pmatrix} \tag{20}$$

The optimal solution to the problem is obtained by applying the Pontryagin maximum principle. The numerical solution optimizes the discretized values of control inputs $\boldsymbol{u} := \boldsymbol{u}(t_i)$ at N equally spaced knot points t_i.

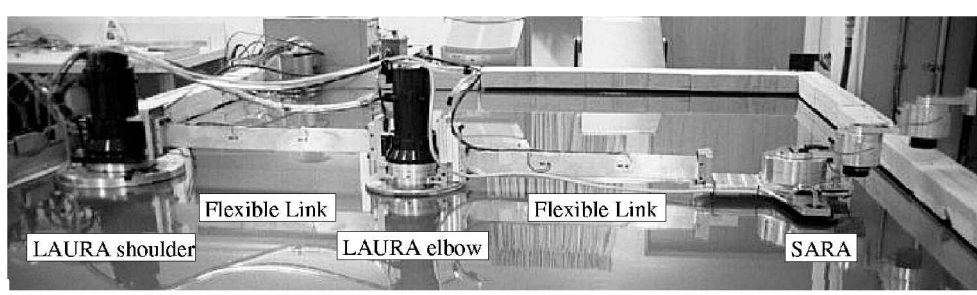

Fig. 2 LAURA–SARA manipulator.

Note that one difficulty arises in plotting the prediction maps described in Sec. II. The maps can be easily plotted for systems with 2-DOF only, for example, a 2-DOF microrobot attached to a macroarm in a locked-joint configuration. For cases with more DOF, the maps are no longer two dimensional, which significantly complicates their use. Inasmuch as it is numerical, the global optimization procedure is not limited by these plotting constraints of the prediction maps and can be used for manipulators with any number of DOF. However, the generality and accuracy of the optimal solution comes at a high computational cost.

In the following two sections, we compare the globally optimal path with respect to the heuristics of the MCM and predictions of the accelerative damping map.

B. MCM Results

Given an MCM for a particular manipulator, a joint path between two configurations to reduce vibration can be chosen by following heuristics analogous to those proposed for the coupling map by Torres and Dubowsky.[15] In particular, we choose the motion along the minimum coupling lines in areas of higher coupling (darkly shaded) and, if necessary, across the minimum coupling lines only in areas of lower coupling. We now compare the global optimization solution with the MCM, for the three example manipulator systems described in Sec. III.

Figure 3 shows the globally optimal path superimposed on the MCM for the REMSPATIAL manipulator. The task is chosen to allow easy identification of the optimal trajectory: Move the joints from (−90, 0) to (90, 0) deg, rest-to-rest, in 5 s. As expected, the globally optimal path first prescribes elbow rotation that orients the flexible link to decouple vibration from shoulder joint rotation. After slewing the shoulder joint, the elbow joint is returned to the desired angle. In this case, the globally optimal path (white thick line) agrees well with MCM, and both methods also agree with our intuition. The instantaneous direction of minimum coupling (along black vertical lines) requires that the elbow rotate while the shoulder does not. Once the joint configuration is in an area of relatively low coupling (lightly shaded region), the joint path crosses the minimum coupling lines.

Results for REMGRAVITY manipulator are shown in Fig. 4. Because gravity is not included in the MCM derivation and the manipulator is identical to the preceding example, the map looks identical to that in Fig. 3. The globally optimal solution is shown for two maneuvers: (−90, 0) to (90, 0) deg, rest-to-rest, in 5 s (white line) and the same in 1 s (black line). We immediately observe that both paths violate the MCM heuristics when gravity dominates the disturbance to the flexible link. For the slow 5-s maneuver (white line), gravity is dominant throughout most of the motion, and hence, the corresponding joint path is in complete discord with the MCM heuristics. The optimal path for the fast maneuver (black line) agrees with the MCM at the beginning and end of the motion when shoulder acceleration dominates. (In Fig. 4, the global solution follows the minimum coupling lines in the dark region in the initial and final stages of the motion.) However, it disagrees in the middle of the motion, when shoulder joint acceleration is zero and gravity dominates.

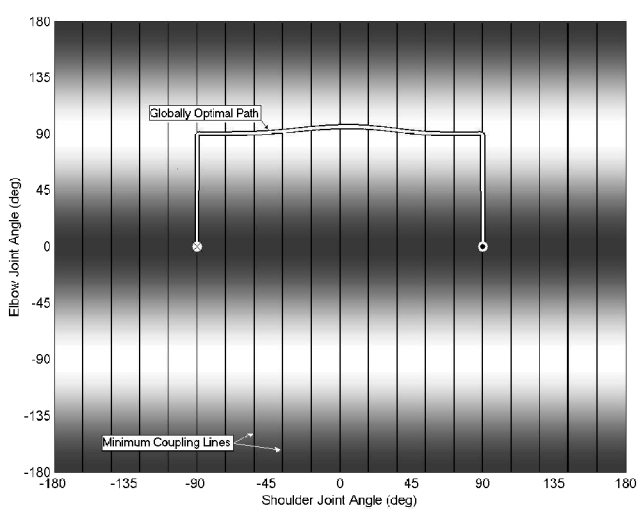

Fig. 3 MCM for REMSPATIAL manipulator with optimal joint path (white thick line) superimposed.

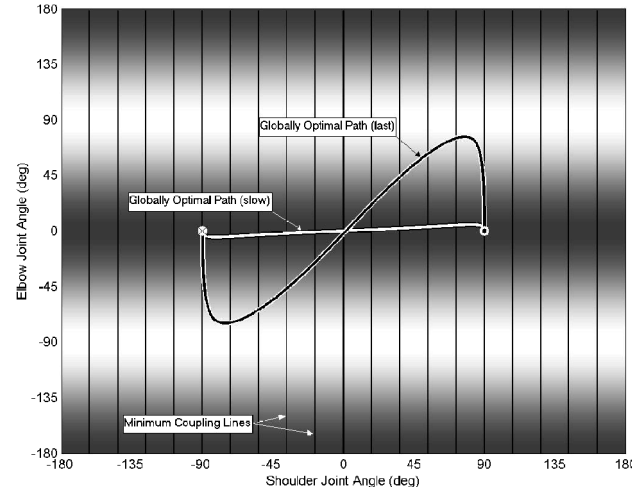

Fig. 4 MCM for REMGRAVITY manipulator with optimal joint paths for slow maneuver (white line) and fast maneuver (black) superimposed.

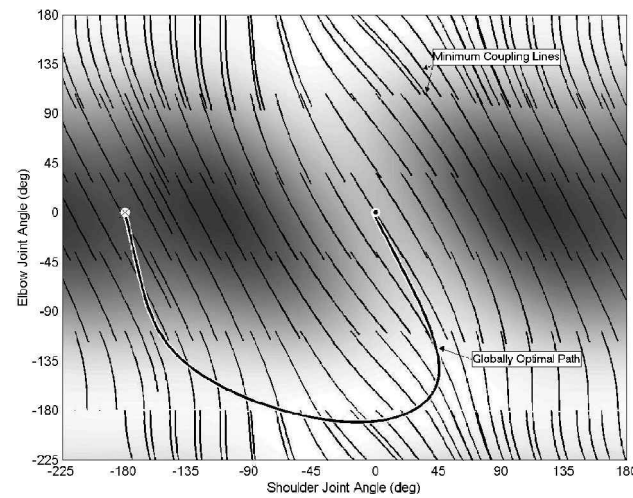

Fig. 5 MCM for LAURA–SARA manipulator with optimal joint path (black line) superimposed.

The MCM and the globally optimal path for the LAURA–SARA manipulator are less intuitive; however, Fig. 5 also shows agreement between the two. The specified point-to-point task was to move SARA's shoulder and elbow joints from (−180, 0) to (0, 0) deg, rest-to-rest, in 1 s. The SARA wrist and two LAURA joints were locked in the 0-deg straight-out configuration. During the trajectory, the elbow joint moves to −180 deg that is, back over the shoulder joint. For this macro–micro manipulator, such motion has the effect of reducing the moment applied to the tip of the macromanipulator as the shoulder joint slews, thus reducing vibration excitation.

C. Accelerative Damping Map Results

The accelerative damping maps for the REMSPATIAL and REMGRAVITY examples look identical to the respective MCM and are not included. The map obtained for the LAURA–SARA manipulators by using the accelerative damping matrix of Eq. (13) is shown in Fig. 6. As can be seen, it looks substantially different from the MCM of Fig. 5; however, there is no obvious contradiction between the map heuristics and the globally optimal solution. In addition to the differences in the configurations predicted for high and low coupling, it appears that the minimum coupling directions are not unique in some places. This is evidenced by the intersection of lines and sharp corners and may occur because the eigenspace corresponding to the minimum eigenvalue is not one dimensional. We have not tackled the problem of how to choose the minimum coupling direction to maintain continuity. The issue of continuity of

eigenvectors has been addressed by Junkins and Schaub,[19] albeit in a different context.

V. Application to Active Damping

The accelerative damping map (ADM) and MIM are both used for the LAURA–SARA manipulator to identify SARA's configuration that produces optimal damping of the supporting macroarm. Predictions of the maps are evaluated against the experimental results obtained with the manipulator. The experiments are conducted with the frequency matching algorithm used for the active damping controller for SARA, described briefly next. Evaluation of alternate active damping controllers is outside the scope of the present paper. It is expected that all feasible controllers will yield better performance when the microrobot is in the optimal configuration.

A. Frequency Matching Algorithm

The frequency matching algorithm[20] is a method of active damping that relies solely on PD control of the micromanipulator joints. Therefore, the control law is of the form

$$\boldsymbol{\tau} = -\boldsymbol{P}_{\mathrm{FM}}(\boldsymbol{q}_r - \bar{\boldsymbol{q}}_r) - \boldsymbol{D}_{\mathrm{FM}}\dot{\boldsymbol{q}}_r \tag{21}$$

where $\bar{\boldsymbol{q}}_r$ is the nominal micromanipulator configuration. The objective of frequency matching is to tune (offline) the micromanipulator PD gains, for a particular nominal configuration, to achieve optimal damping of the dominant mode of vibration of the macroarm. Thus, the derivative gains are determined to maximize the rate of energy dissipation, which in turn is achieved by matching micromanipulator closed-loop frequencies to $\bar{\omega}_e$. The proportional gains are chosen as a tradeoff between damping performance and closed-loop response of the microjoints. This results in the following gain matrices[20]:

$$\boldsymbol{P}_{\mathrm{FM}} = \bar{\omega}_e^2 \boldsymbol{M}_{rr}, \qquad \boldsymbol{D}_{\mathrm{FM}} = 2\zeta\bar{\omega}_e \boldsymbol{M}_{rr} \tag{22}$$

Note that the gain matrices of the frequency matching control law are symmetric positive definite. Therefore, stability of the resulting controller is guaranteed by the constant setpoint $\bar{\boldsymbol{q}}_r$ (Ref. 21).

B. ADM and MIM Results

The ADM and the MIM were obtained for the experimental LAURA–SARA manipulator and are included in Fig. 7. Surface plots are used here rather than the contour plots used earlier in Sec. IV because they are more suitable for the active damping application. The peaks correspond to the dark region in the contour plots (high coupling). The maps were computed with SARA wrist locked in the straight-out configuration, whereas LAURA's elbow joint is locked at 60 deg (Fig. 8).

Note from Fig. 7 that the two maps are very similar in shape: Both maps have a complex structure that is strongly dependent on the nominal angles of both the SARA base and elbow joints. The primary difference is that the central peak is more prominent in the ADM. Both maps predict peak active damping performance near $\bar{\theta}_{S1} = \bar{\theta}_{S2} = 0$.

To validate the predictions of the two maps, a series of experiments were conducted with the LAURA–SARA arm. Briefly, the experimental procedure involved the following steps. At the start of each experiment, LAURA was deployed to the test configuration, as shown in Fig. 8, with SARA controlled by stiff PD gains. SARA's PD gains were switched to appropriate frequency matching gains for active damping 2 s after the deployment maneuver. A detailed description of the experimental procedure may be found by Van Vliet.[16] These experiments were repeated for a grid of nominal

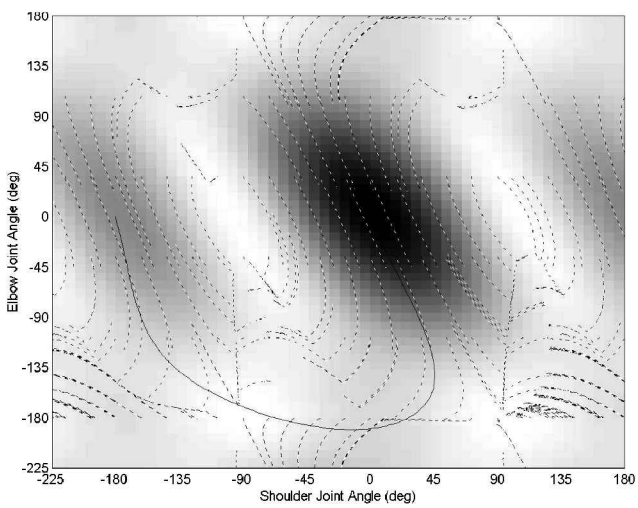

Fig. 6 ADM for LAURA–SARA manipulator with ——, optimal joint path, superimposed.

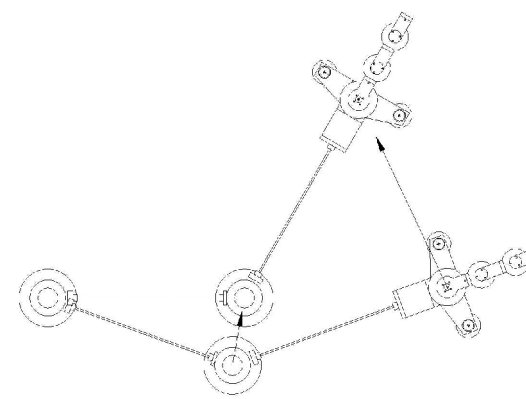

Fig. 8 LAURA–SARA configuration and deployment maneuver.

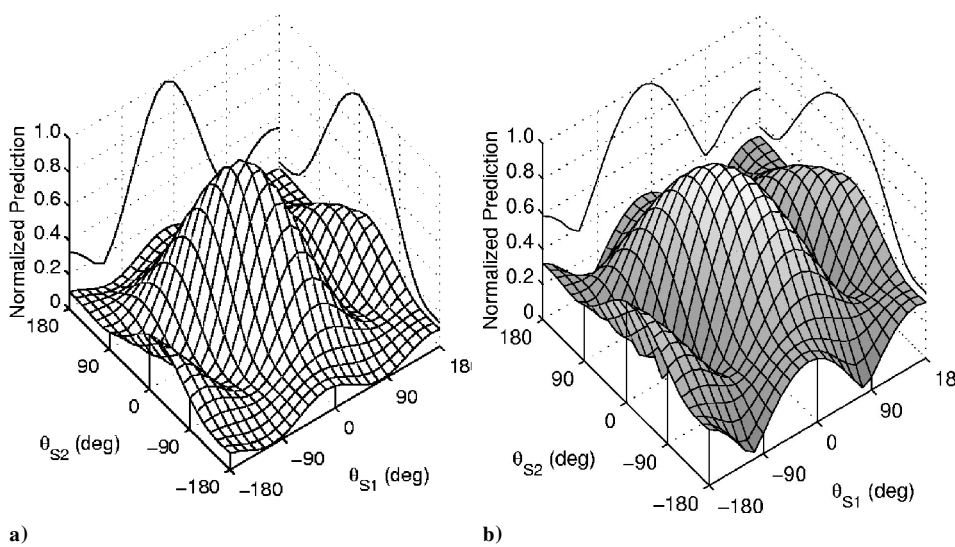

Fig. 7 LAURA–SARA manipulator: a) normalized ADM and b) MIM.

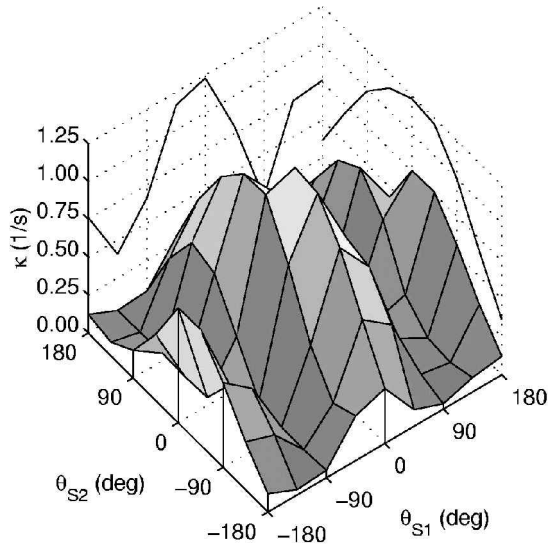

Fig. 9 Observed damping performance on LAURA–SARA manipulator.

SARA configurations with its base and elbow angles incremented at 45 deg. SARA's third joint was locked in all experiments.

The data from each experiment were analyzed offline to determine the rate of decay κ of the strain energy in the macroarm. The strain energy was calculated from strain measurements of LAURA's flexible links. Figure 9 shows the measured damping performance κ over the complete range of SARA base and elbow joint angles. A comparison of the measured damping performance with the predicted performance of the two maps in Fig. 7 indicates very good correlation between predictions and measurements, with MIM consistently proving a slightly better predictor of the experimental damping than ADM. Similar results and conclusions were obtained for a different (locked) configuration of the LAURA manipulator.

VI. Conclusions

We presented three novel predictive tools for motion planning and active damping problems. For the former, the MCM and the ADM can be used to determine the joint motions or paths in joint space, which minimize vibration excitation of the flexible manipulator. The MCM is based on the coupling map concept developed previously, but is applicable to general flexible manipulators. The motivation for devising the maps is to enable trajectory (path) planning for minimal vibration in a real-time environment.

For the simple example manipulator considered in the paper, the two maps for motion planning are nearly identical. For the more complicated system, the LAURA–SARA manipulator, the maps differ, but both could predict a path similar to that calculated with the numerical globally optimal solution. The maps fail when applied to the example manipulator in a gravitational environment because their derivations do not take into account external disturbance: The map heuristics predict suitable joint paths when the joint motions represent the dominant vibration disturbance throughout the maneuver. When this is taken into account, comparison of the paths predicted with the maps to those calculated with the globally optimal motion planner shows a good agreement between the two procedures.

In the active damping scenario, the ADM and the MIM allow identification of micromanipulator nominal configurations that, in some sense, provide the most effective damping of the macroarm vibrations. It was gratifying to observe that even for a complex macro–micro manipulator, such as LAURA–SARA, the two maps are very similar to each other. Furthermore, the predictions of the maps were supported with the experimentally measured damping performance of the LAURA–SARA manipulator system. Based on our results, we conclude that the proposed maps can provide reliable and computationally inexpensive tools for motion planning and active damping problems for space-based manipulator systems. Further research is required to prove these map concepts for more complicated spatial manipulator systems.

Acknowledgments

The authors acknowledge the Natural Sciences and Engineering Research Council for its support under the Research Grant and Equipment Grant programs.

References

[1]Mohri, A., Sarkar, P. K., and Yamamoto, M., "An Efficient Motion Planning of Flexible Manipulator Along Specified Path," *Proceedings of the 1998 IEEE International Conference on Robotics and Automation*, IEEE Publications, New York, 1998, pp. 1104–1109.

[2]Tu, Q., and Rastegar, J., "Manipulator Trajectory Synthesis for Minimal Vibrational Excitation Due to the Payload," *Transactions of the CSME*, Vol. 17, No. 4A, 1993, pp. 557–566.

[3]Kim, W., and Rastegar, J., "Robot Manipulator Trajectory Synthesis for Minimal Vibrational Excitation," *Proceedings of 1997 ASME DETC* [CD-ROM], DETC97/VIB4130, American Society of Mechanical Engineers, Fairfield, NJ, Sept. 1997.

[4]Liu, K., and Kujath, M. R., "Trajectory Optimization for a Two-link Flexible Manipulator," *International Journal of Robotics and Automation*, Vol. 11, No. 2, 1996, pp. 56–61.

[5]Yao, C.-M., and Cheng, W.-H., "Joint Space Trajectory Planning for Flexible Manipulators," *Journal of Robotic Systems*, Vol. 12, No. 5, 1995, pp. 287–299.

[6]Torres, M. A., Dubowsky, S., and Pisoni, A. C., "Path-planning for Elastically-mounted Space Manipulators: Experimental Evaluation of the Coupling Map," *Proceedings of the 1994 IEEE International Conference on Robotics and Automation*, IEEE Computer Society Press, Los Alamitos, CA, 1994, pp. 2227–2233.

[7]Book, W. J., and Lee, S. H., "Vibration Control of a Large Flexible Manipulator by a Small Robotic Arm," *Proceedings of the American Control Conference*, American Automatic Control Council, Green Valley, AZ, 1989, pp. 1377–1380.

[8]Lee, S. H., and Book, W. J., "Robot Vibration Control Using Inertial Damping Forces," *Proceeding of VIII CISM–IFToMM Symposium on the Theory and Practice of Robots and Manipulators*, International Centre for Mechanical Sciences, Udine, Italy, July 1990.

[9]Trudnowski, D. J., Baker, C. P., and Evans, M. S., "Damping Control of Large Flexible Manipulator Through Inertial Forces of a Small Manipulator," *Proceedings of the American Control Conference*, American Automatic Control Council, Evanston, IL, 1993, pp. 2878, 2879.

[10]Lew, J. Y., and Trudnowski, D. J., "Vibration Control of a Micro/Macro-Manipulator System," *IEEE Control Systems Magazine*, Vol. 16, No. 1, 1996, pp. 26–31.

[11]Cannon, D. W., Magee, D. P., Book, W. J., and Lew, J. Y., "Experimental Study on Micro/Macro Manipulator Vibration Control," *IEEE International Conference on Robotics and Automation*, Pt. 3, IEEE Publications, New York, 1996, pp. 2549–2554.

[12]Sharf, I., "Active Damping of a Large Flexible Manipulator with a Short-Reach Robot," *Journal of Dynamic Systems Measurement and Control*, Vol. 118, No. 4, 1996, pp. 704–713.

[13]Book, W. J., and Loper, J. C., "Inverse Dynamics for Commanding Micromanipulator Inertial Forces to Damp Macromanipulator Vibration," *IEEE International Conference on Intelligent Robots and Systems*, Vol. 2, IEEE Publications, Piscataway, NJ, 1999, pp. 707–714.

[14]Torres, M. A., Dubowsky, S., and Pisoni, A. C., "Vibration Control of Deployment Structures' Long-Reach Space Manipulators: The P-PED Method," *IEEE International Conference on Robotics and Automation*, IEEE Publications, New York, 1996, pp. 2498–2504.

[15]Torres, M. A., and Dubowsky, S., "Path-planning for Elastically Constrained Space Manipulator Systems," *Proceedings of the 1993 IEEE International Conference on Robotics and Automation*, Vol. 1, IEEE Computer Society Press, Los Alamitos, CA, 1993, pp. 812–817.

[16]Van Vliet, C. J., "Predicted and Observed Active Damping Performance of Macro–Micro Manipulators," M.Sc. Thesis, Dept. of Mechanical Engineering, Univ. of Victoria, Victoria, BC, Canada, 1998.

[17]Van Vliet, J., and Sharf, I., "Development of a Planar Macro–Micro Manipulator Facility: From Design Through Model Validation," *Canadian Aeronautics and Space Journal*, Vol. 44, No. 1, 1998, pp. 40–50.

[18]Pond, B., and Sharf, I., "Experimental Evaluation of Flexible Manipulator Trajectory Optimization," *Journal of Guidance, Control, and Dynamics*, Vol. 24, No. 4, 2001, pp. 834–843.

[19]Junkins, J. L., and Schaub, H., "Orthogonal Square Root Eigenfactor Parameterization of Mass Matrices," *Journal of Guidance, Control, and Dynamics*, Vol. 20, No. 6, 1997, pp. 118–1124.

[20]Van Vliet, J., and Sharf, I., "A Frequency Matching Algorithm for Active Damping of Macro–Micro Manipulator Vibrations," *Proceedings of the 1998 IEEE/RSJ International Conference on Intelligent Robots and Systems*, Vol. 2, IEEE Publications, Piscataway, NJ, 1998, pp. 782–787.

[21]Yoshikawa, T., *Foundations of Robotics*, MIT Press, Cambridge, MA, 1990.